Marine Structures 90 (2023) 103441

Contents lists available at ScienceDirect

Marine Structures

journal homepage: www.elsevier.com/locate/marstruc

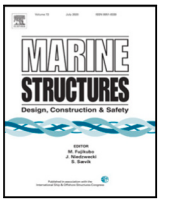

Dynamic analysis of a dual-spar floating offshore wind farm with shared moorings in extreme environmental conditions

Guodong Liang [a,*], Zhiyu Jiang [a], Karl Merz [b]

[a] Department of Engineering Sciences, University of Agder, N-4898 Grimstad, Norway
[b] SINTEF Energy Research, N-7034 Trondheim, Norway

ARTICLE INFO

Keywords:
Floating offshore wind farm
Shared mooring system
Dynamic response
Time-domain simulation
Extreme response
Wind and waves

ABSTRACT

The concept of a shared mooring system was proposed to reduce mooring and anchoring costs. Shared moorings also add complexity to the floating offshore wind farm system and pose design challenges. To understand the system dynamics, this paper presents a dynamic analysis for a dual-spar floating offshore wind farm with a shared mooring system in extreme environmental conditions. First, a numerical model of the floating offshore wind farm was established in a commercial simulation tool. Then, time-domain simulations were performed for the parked wind farm under extreme wind and wave conditions. A sensitivity study was carried out to investigate the influence of loading directions and shared line mooring properties. To highlight the influence of the shared line, the results were compared to those of a single spar floating wind turbine, and larger platform motions and higher tension loads in single lines are observed for the wind farm with shared moorings. The loading direction affects the platform motions and mooring response of the floating offshore wind farm. Comparing the investigated loading directions to the 0-deg loading direction, the variation of mean mooring tension at the fairlead is up to 84% for single lines and 16% for the shared line. The influence of the shared line properties in the platform motions and the structural responses is limited. These findings improve understanding of the dynamic characteristics of floating offshore wind farms with a shared mooring system.

1. Introduction

A floating offshore wind farm (FOWF) is a promising solution to the growing demand for clean and de-carbonized energy. The design concept of a shared mooring system has been proposed to reduce the cost of FOWFs [1]. A shared mooring system can consist of single lines and shared lines without additional mooring elements. In such a case, each single line connects a floating offshore wind turbine (FOWT) to the anchor, and a shared line connects two adjacent FOWTs directly and is completely hanging in the water. Top views of shared mooring systems for pilot-scale FOWFs are presented in Fig. 1, in which each FOWT is connected to three mooring lines. Fewer mooring lines and anchors are required for an FOWF with a shared mooring system, which indicates potential for cost-saving. However, unlike conventional FOWFs, e.g., Hywind Scotland [2], where each FOWT is separate, the novel FOWFs with shared moorings are expected to exhibit different dynamic response behavior under environmental loading. The technical feasibility of such a concept needs to be studied through detailed investigations of the system's dynamic characteristics.

Goldschmidt and Muskulus [3] studied the dynamic properties of FOWFs with shared mooring systems using simplified models for several configurations. The cost-saving potential of the shared mooring system was revealed but increasing requirements for

* Corresponding author.
E-mail addresses: guodong.liang@uia.no (G. Liang), zhiyu.jiang@uia.no (Z. Jiang), inducedvelocity@gmail.com (K. Merz).

https://doi.org/10.1016/j.marstruc.2023.103441
Received 11 May 2022; Received in revised form 23 January 2023; Accepted 27 February 2023
Available online 2 May 2023

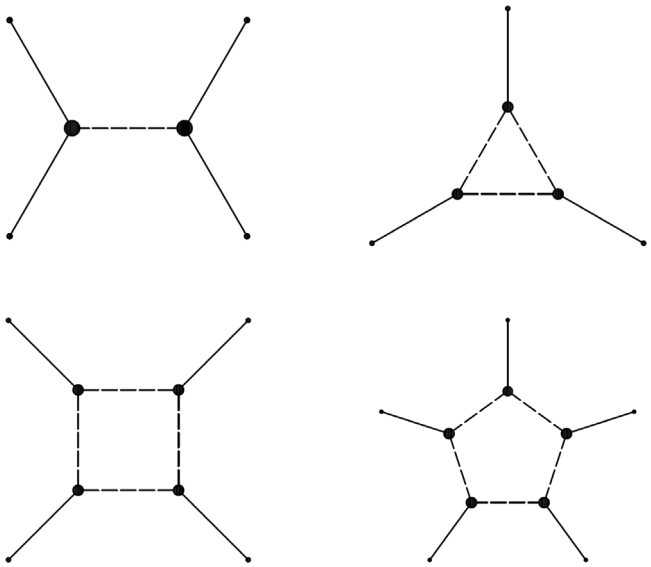

Fig. 1. Shared mooring systems for pilot-scale FOWFs (large solid circle: FOWT, small solid point: anchor, solid line: single line, dashed line: shared line).

the mooring system were reported with larger farm size. Hall and Connolly [4] investigated the dynamics of a four-turbine square-shaped FOWF with semi-submersible FOWTs and a shared mooring system. Complex restoring properties and a greater tendency for resonance were found for the mooring systems with shared lines. In a follow-up study by Connolly and Hall [5], a simplified design algorithm was proposed for the preliminary sizing of shared mooring systems for pilot-scale FOWFs. Several layouts of shared mooring systems were designed and analyzed for a four-turbine FOWF in different water depths. In [6], Hall modeled and studied the mooring failure scenario of a dual-semi-submersible FOWF in time-domain simulations. Wilson et al. [7] proposed a design optimization approach based on a linearized method to model the force-horizontal displacement relationship of FOWTs with a shared mooring system. The design approach was based on quasi-static mooring analysis and applied to different layouts of FOWFs. Munir et al. [8] studied the dynamic behavior of a dual-semi-submersible FOWF with a shared mooring system and considered two different turbine spacings. The study only examined the platform motions. Liang et al. [9] applied the theory of elastic catenary of hanging cable structures to model the shared line. In a follow-up study, Liang et al. [10] studied the influence of the shared mooring system on the natural periods and natural modes of a dual-spar FOWF.

The dynamic response of an FOWF in extreme environmental conditions is important to the survivability and structural integrity of the system. To the authors' knowledge, there is a lack of literature addressing this aspect for FOWFs with shared moorings. To explore the extreme responses of FOWFs with shared moorings, we study the dynamic behaviors of a baseline FOWF with two FOWTs, one shared line, and four single lines for a deep-water site. The influence of the shared line is investigated by comparing the structural and motion response statistics of the FOWF with those of a single FOWT under extreme wind and wave conditions. To elucidate the dynamic characteristics of the FOWF, we further consider different loading directions and shared line properties in a sensitivity study. In the following, the baseline FOWF is introduced in Section 2. The procedures of numerical modeling are described in Section 3. Section 4 presents the details of the case study. The results are analyzed and discussed in Section 5. Finally, conclusions are summarized in Section 6.

2. Concept description of the baseline FOWF

The dual-spar baseline FOWF is illustrated in Fig. 2. As shown, two OC3 Hywind spar FOWTs [11,12], Spar 1 and Spar 2, are deployed in the global surge direction, i.e., along the x_g-axis. Table 1 presents some of the main design parameters of the OC3 Hywind spar FOWT. The turbine spacing is 1000 m in the initial configuration, which is approximately eight times the rotor diameter.

The FOWTs are connected by a shared line, Line 5, in the x_g direction. Due to its self weight, the shared line is pre-tensioned and has a catenary line shape; see Fig. 3. As a result, two FOWTs move towards each other along the x_g-axis by a short distance under static equilibrium. Each FOWT has two single lines which are attached to the seabed through anchors. The projected angle between any two adjacent mooring lines is 120 deg.

The draft of fairleads and the radius from the fairleads to the corresponding floater centerlines are kept the same as in [12]. All fairleads of single lines and the shared line are located 70 m below the still water level (SWL) and 5.2 m away from the corresponding floater centerlines. The water depth is 320 m below the SWL. The radius from floater centerlines to corresponding anchors is increased to 953.87 m. A mooring design is made for a single OC3 Hywind spar FOWT in [10]. A two-segment design with chain and wire is used as it is more representative of actual mooring lines than that of the one-segment design. Detailed design

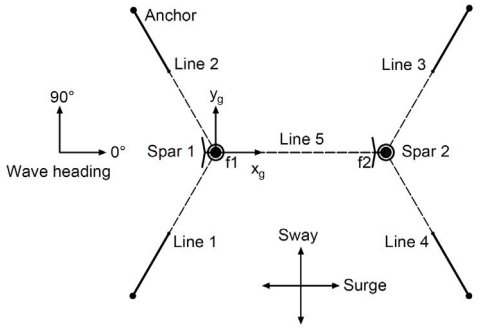

(a) Top view

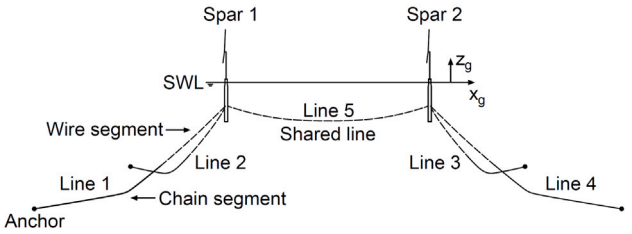

(b) Side view

Fig. 2. Illustration of the dual-spar baseline FOWF (SWL: still water level, dashed line: wire, solid line: chain).

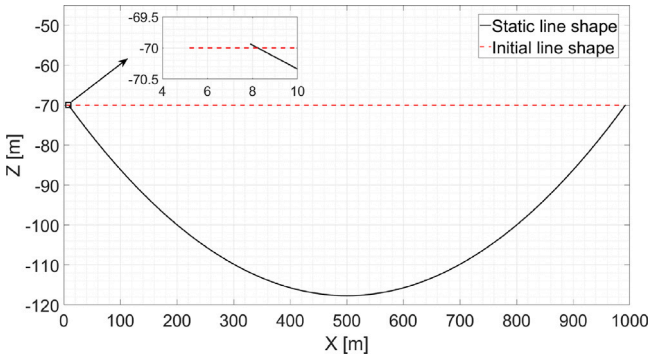

Fig. 3. Static line shape of the shared line of the dual-spar baseline FOWF (loading direction: 0 deg).

Table 1
Main design parameters of the OC3 Hywind Spar FOWT [11,12].

Design parameter	Value
Rated power capacity [MW]	5
Turbine type [–]	Upwind, 3 blades
Cut-in, rated, cut-out wind speed [m/s]	3, 11.4, 25
Rotor diameter [m]	126
Hub height [m]	90
Total draft [m]	120
Number of mooring lines [–]	3
Radius to fairleads from floater centerline [m]	5.2
Depth to fairleads below SWL [m]	70
Angle between adjacent lines [deg]	120
Water depth [m]	320

Table 2
Mooring properties of the baseline FOWF.

Mooring properties	Single line		Shared line
	Chain segment	Wire segment	
Material	R3 studless chain	Steel wire rope	Steel wire rope
Water depth [m]	320	320	320
Unstretched length [m]	550	452.2	989.6
Diameter [mm]	115	90	90
Sheath thickness [mm]	–	10	10
Mass density [kg/m]	264.50	42.77	42.77
Weight in water [N/m]	2385.86	324.00	324.00
Extensional stiffness [N]	1.06E+09	7.64E+08	7.64E+08
Minimum breaking strength [N]	1.03E+07	8.38E+06	8.38E+06

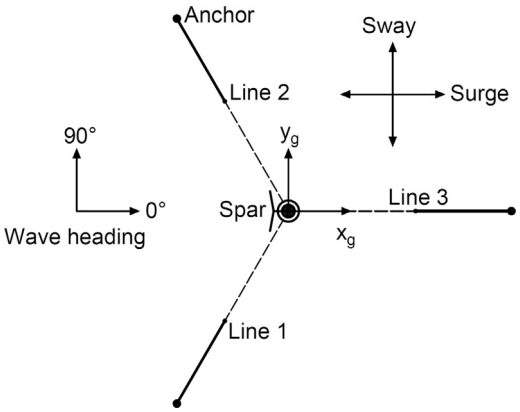

Fig. 4. Top view of the single FOWT (dashed line: wire, solid line: chain).

procedures can be found in [10]. The mooring design is applied to the single lines of the baseline FOWF. As shown in Fig. 2(b), the upper segment is made of wire and the lower segment is made of mooring chain. The shared line is supposed to be suspended and submerged in the water all the time without touching the sea bed or interfering with ship traffic. Wire is lighter than chain and is therefore used for the shared line. Because there is no design recommendation for the shared line, wire properties of the single lines are used for the shared line for simplicity. Mooring properties of the baseline FOWF are summarized in Table 2.

To investigate the influence of the shared line, a single spar FOWT is modeled as well. As illustrated in Fig. 4, the three single lines of the FOWT have the same orientations as Spar 1 in the baseline FOWF. The partial safety factors for an FOWF are not calibrated in the mooring design standards [13], so the configurations of the single lines are kept the same for the baseline FOWF and the single FOWT for comparison.

3. Numerical modeling of the dual-spar FOWF

To perform dynamic analyses, the baseline FOWF and the single FOWT described in Section 2 are modeled in SIMA [14,15] in which the OC3 Hywind spar FOWTs are modeled according to [11,12].

A hydrodynamic analysis is performed for the panel model of the single spar in the frequency domain using the potential-flow program WADAM [16] to obtain hydrodynamic properties, like the frequency-dependent hydrodynamic added mass and radiation damping coefficients, the first-order wave force transfer functions, the second-order mean wave drift forces.

The spar floaters are modeled as rigid bodies in the SIMO module of SIMA. Six degrees of freedom (DOFs) of the rigid-body motions are considered for each FOWT, namely, surge, sway, heave, roll, pitch and yaw. Mooring lines of the baseline FOWF are modeled as slender structures in the RIFLEX module of SIMA. Fifty bar elements with the same cross-section properties are used to model the chain segment and the wire segment of the single lines, respectively. One hundred bar elements are used to model the shared line. Detailed failure modes of mooring materials, e.g., wear of chain or birdcaging of wire, are not considered in the numerical modeling of the mooring system. The same modeling method is applied to model the single FOWT in SIMA.

The equation of motion for the floating system can be written in the time domain as:

$$(\mathbf{M}+\mathbf{A}_{\infty})\ddot{\mathbf{x}}+\mathbf{B}_1\dot{\mathbf{x}}+\mathbf{B}_2\dot{\mathbf{x}}|\dot{\mathbf{x}}|+\mathbf{C}\mathbf{x}+\int_0^t \mathbf{h}(t-\tau)\dot{\mathbf{x}}(\tau)d\tau=\mathbf{f}(t,\mathbf{x},\dot{\mathbf{x}}) \tag{1}$$

in which $\mathbf{M}$ is the structural mass matrix; $\mathbf{A}_{\infty}$ is the added mass matrix at infinite frequency; $\mathbf{B_1}$ is the matrix of linear damping coefficients; $\mathbf{B_2}$ is the matrix of quadratic damping coefficients; $\mathbf{C}$ is the matrix of restoring coefficients; $\mathbf{h}(\tau)$ is the retardation

Table 3
Natural periods of the baseline FOWF and the single FOWT [s].

DOF		Surge	Sway	Heave	Roll	Pitch	Yaw
Baseline FOWF	Mode 1	135.51	76.25	31.13	29.48	29.47	8.36
	Mode 2	63.52	75.64	31.03	29.48	29.46	8.34
Single FOWT		79.65	79.64	30.75	29.31	29.31	8.69

Table 4
Environmental parameters for the extreme environmental conditions.

Parameter	Value
U_w (at hub-height) [m/s]	42.71
I [–] (Turbulence intensity)	0.12
H_s [m]	15.50
T_p [s]	14.45

function; $\mathbf{x}$, $\dot{\mathbf{x}}$, and $\ddot{\mathbf{x}}$ are the vectors of the displacement, velocity and acceleration in the time domain; $\mathbf{f}$ is the external force vector. Hydrodynamic properties obtained from WADAM are implemented in the SIMA model of the baseline FOWF to calculate wave loads. Wave forces are integrated to the mean water level. Morison elements are added to the underwater part of the spar floaters to calculate the drag forces. The hydrodynamic coupling between two FOWTs is ignored because of the large turbine spacing. In extreme environmental conditions, the FOWTs are parked (standing still) and the blades are feathered. As found in [17], the extreme response of the baseline FOWF is not entirely wave-dominant and aerodynamic loads do play a role in extreme conditions. Therefore, aerodynamic loads acting on the FOWTs are considered in extreme environmental conditions. The airfoil coefficients of the FOWT blades specified in [11] are used, based on which the aerodynamic loads are calculated. Drag coefficients are specified to consider the drag force acting on the tower. According to the offshore standard [18], the drag coefficients are set to 0.65 based on the Reynolds number calculation. Since two FOWTs are in a parked condition with rotors at standstill, the aerodynamic interaction effect between the FOWTs is ignored.

Twelve free decay tests are performed for the baseline FOWF and six free decay tests are performed for the single FOWT in SIMA. For the FOWF, forces or moments are applied to the FOWTs to obtain initial displacements or rotations in the corresponding DOFs. Then the FOWTs are released and oscillate in the still water. As studied in [10], the baseline FOWF has twelve natural modes and natural periods. The estimated natural periods of the baseline FOWF and the single FOWT are summarized in Table 3. For the FOWF, two natural modes, Mode 1 and Mode 2, are identified for all six DOFs. Mode 1 indicates that the two FOWTs move in the same direction and Mode 2 indicates that they move in opposite directions. From Table 3, it is seen that the natural periods of translational DOFs in the horizontal plane are mostly influenced by the presence of the shared line, i.e., in the surge and sway directions, because the diagonal terms of stiffness matrix in these two directions only have contributions from mooring stiffness [10].

4. Case study

A case study is conducted to investigate the dynamic characteristics of the baseline FOWF in extreme environmental conditions. First, the influence of the shared mooring on the FOWTs is demonstrated by comparing the dynamic responses to those of the single FOWT. Then, the influence of loading directions and shared line diameters are further explored for the baseline FOWF.

4.1. Metocean condition

In accordance with the offshore standard [19], the extreme environmental conditions are determined with a return period of 50 years. The metocean condition of a European offshore site, "Norway 5" [20], is used. The 50-year environmental contour surface is calculated based on the joint distribution of the mean wind speed (U_w), the significant wave height (H_s) and the spectral peak period (T_p). The sea state on the contour surface with the highest H_s is selected. Other environmental loads like current are not considered in this study. The wind turbine Class I-B and the IEC Normal Turbulence Model are chosen [21,22]. The environmental parameters are listed in Table 4.

Turbulent wind and irregular waves are considered in simulations. The wind and waves are assumed to come in the same direction and are specified by a parameter, the loading direction. In SIMA, irregular waves are generated with random wave seeds. Turbulent wind fields are simulated in Turbsim [23] and used in SIMA. The size of the turbulent wind fields is determined to ensure that the FOWTs stay inside during motions.

4.2. Dynamic analysis of the baseline FOWF

To study how the dynamic characteristics of the FOWTs are influenced by the shared line, dynamic analyses are performed for the baseline FOWF and the single FOWT under the extreme environmental conditions described in Section 4.1. Two loading directions, 0 deg and 90 deg, are considered; see Figs. 2(a) and 4.

Table 5
Mooring properties for different shared line diameters in the sensitivity study.

Diameter [mm]	90	100	110	120	130
Mass density [kg/m]	42.77	52.24	62.65	73.98	86.25
Weight in water [N/m]	324.00	398.75	481.09	571.00	668.44
Cross-sectional area [m^2]	0.0095	0.0113	0.0133	0.0154	0.0177
Extensional stiffness [N]	7.64E+08	9.35E+08	1.12E+09	1.32E+09	1.54E+09
Minimum breaking strength [N]	8.38E+06	1.04E+07	1.25E+07	1.49E+07	1.76E+07

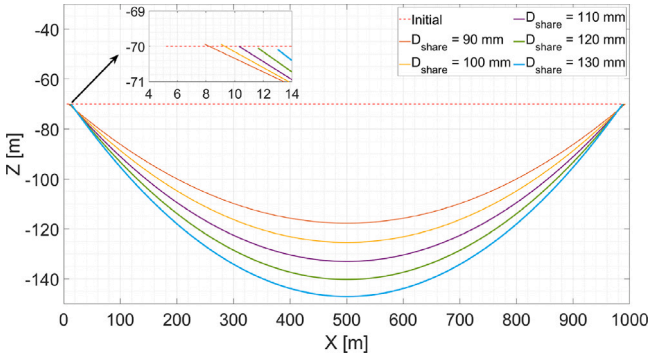

Fig. 5. Static line shape of the shared line in the sensitivity study of the shared line diameter (loading direction: 0 deg).

To determine the number of realizations for the dynamic analyses, a convergence study was conducted with the 0-deg loading direction. Platform motions and structural responses of the baseline FOWF are considered. The results show that twenty one-hour realizations are sufficient for the extreme response statistics to reach convergence. Therefore, for each considered environmental condition, twenty one-hour time-domain simulations were performed for the baseline FOWF and the single FOWT.

4.3. Sensitivity study

4.3.1. Sensitivity study on the loading direction

A sensitivity study is conducted for the loading direction to investigate how it will influence the dynamic behavior of the baseline FOWF. Because of the symmetry of the dual-spar configuration, we select four loading directions, 0 deg, 30 deg, 60 deg and 90 deg. For each loading direction, 20 one-hour time-domain simulations are performed. The results of platform motions and structural responses are analyzed and compared.

4.3.2. Sensitivity study on the shared line diameter

To investigate the influence of the shared line on the system's dynamic characteristics, various shared line mooring properties are investigated as well. Based on the catalogue data of wires, four shared line diameters are selected besides the original shared line diameter for the baseline FOWF. The mooring properties of different shared line diameters are listed in Table 5. The length of the shared line is kept unchanged. The static line shapes of the shared line are plotted in Fig. 5 for different shared line diameters. With an increasing shared line diameter, the shared line is heavier and therefore, the horizontal displacements of FOWTs from their initial positions are larger and so does the sagging depth of the shared line in static equilibrium. Two loading directions, 0 deg and 90 deg, are considered in this sensitivity study. For each loading direction, twenty one-hour time-domain simulations are performed for every configuration with a different shared line diameter and the simulation results are post-processed.

5. Results and discussion

Simulation results obtained from the case study in Section 4 are analyzed and discussed in this section. In Section 5.1, dynamic behaviors of the baseline FOWF are first analyzed and presented through a comparison to the single FOWT in terms of the linearized mooring stiffness, the horizontal platform motions and selected structural responses. Then, results of the sensitivity study are presented in Section 5.2 in which the linearized mooring stiffness, the horizontal platform motions of FOWTs and the selected structural responses are compared step by step. In the following sections, "Spar 1" and "Spar 2" refer to the FOWTs in the dual-spar configuration; see Fig. 2. "Spar" refers to the single FOWT; see Fig. 4.

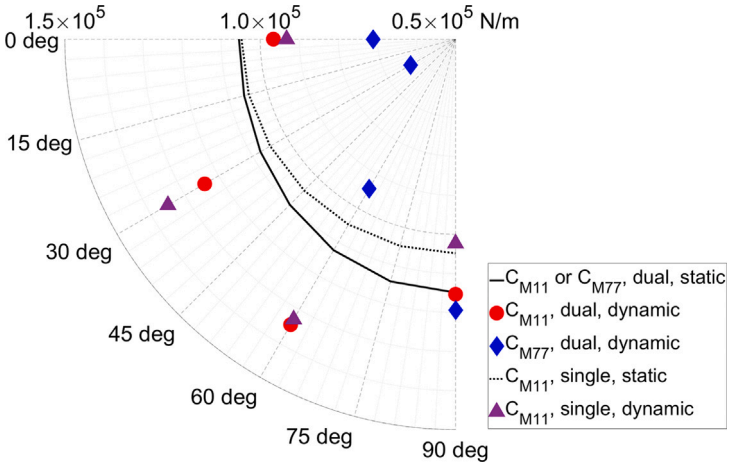

Fig. 6. Linearized mooring stiffness with respect to different loading directions (dual: baseline FOWF, single: single FOWT, static: linearized around the static equilibrium position, dynamic: linearized around the mean dynamic position).

Table 6
Results of horizontal platform motions of FOWTs in the dynamic analysis.

Parameter	Baseline FOWF		Single FOWT
	Spar 1	Spar 2	Spar
Loading direction = 0 deg			
Platform, static equilibrium position [m]	(2.56, 0)	(997.70, 0)	(0,0)
Platform, mean dynamic position [m]	(13.59, 0.35)	(1006.25, 3.71)	(5.28, 0.37)
Platform, motion range[a] [m]	[−12.40, 12.90]	[−12.76, 12.95]	[−11.98, 11.94]
Platform, motion SD[b] [m]	3.64	3.83	3.43
Loading direction = 90 deg			
Platform, static equilibrium position [m]	(2.38, 0.07)	(997.50, 0.07))	(−0.08, 0.08)
Platform, mean dynamic position [m]	(1.95, 11.36)	(996.79, 11.09)	(−1.33, 12.06)
Platform, motion range [m]	[−12.72, 13.61]	[−12.94, 13.16]	[−12.98, 13.72]
Platform, motion SD [m]	3.88	3.82	3.91

[a]"Platform, motion range" refers to the planar platform motions projected in the $x_g - y_g$ plane and along the loading direction. It is calculated with regard to the "Platform, mean dynamic position".
[b]"Platform, motion SD" stands for the standard deviation of the planar platform motions projected in the loading direction.

5.1. Comparison between the baseline FOWF and the single FOWT

5.1.1. Comparison of linearized mooring stiffness

The method presented in [10] is applied to calculate the linearized mooring stiffness of the baseline FOWF and the single FOWT. Both the static equilibrium positions and the mean dynamic positions of the system are taken as the reference position for linearization. The mooring stiffness is linearized in the coordinate system where the x-axis is along the loading direction. The results are plotted in Fig. 6. For the baseline FOWF, the stiffness terms C_{M11} and C_{M77} are the diagonal terms in the linearized mooring stiffness matrix and relate to the motions of Spar 1 and Spar 2 in the loading direction. For the single FOWT, the stiffness terms C_{M11} relate to the motion of Spar in the loading direction.

As shown in Fig. 6, for the baseline FOWF, the stiffness terms "C_{M11}, dual, static" and "C_{M77}, dual, static" experience large changes when the loading direction varies from 0 deg to 90 deg, which is caused by the asymmetry of the shared mooring layout. The stiffness term "C_{M11}, single, static" is insensitive to loading directions due to the symmetry of the mooring layout. For both configurations, the mooring stiffness terms linearized around the mean dynamic position differ from those linearized around the static equilibrium position.

5.1.2. Comparison of platform motion in the horizontal plane

To maintain the structural integrity of power cables and the operation of FOWTs, the motion of FOWTs in the horizontal plane must be limited by the mooring system. Though there is no specific recommendation in the design standards, e.g., [19], an excursion limit as a function of the water depth can be assumed [24]. On the other hand, to utilize the space efficiently, the turbine spacing of an FOWF is not very large in practice. Due to the wake effects, the turbine spacing will influence the power output of wind turbines in a wind farm [25]. Therefore, it is of interest to check the horizontal platform motions of FOWTs.

Platform motions are presented in the global coordinate system. The statistics of horizontal platform motions are shown in Table 6 for the baseline FOWF and the single FOWT, where the ensemble average of the 20 realizations is presented. From Table 6,

Table 7
Results of mooring response in the dynamic analysis.

Parameter	Baseline FOWF			Single FOWT		
	Line 1	Line 2	Line 5 f1	Line 1	Line 2	Line 3
Loading direction = 0 deg						
Pretension [N]	9.50E+05	9.50E+05	8.39E+05	8.50E+05	8.50E+05	8.44E+05
Mooring tension, max [N]	2.34E+06	2.17E+06	5.35E+06	2.04E+06	1.77E+06	1.51E+05
Mooring tension, mean [N]	1.39E+06	1.36E+06	9.61E+05	1.03E+06	9.93E+05	6.86E+05
Mooring tension, SD [N]	1.80E+05	1.76E+05	6.63E+05	1.57E+05	1.43E+05	1.38E+05
Mooring angle, max [deg]	67.43	67.01	90.00	65.94	65.18	64.94
Mooring angle, mean [deg]	63.39	63.19	80.34	61.05	60.77	57.55
Mooring angle, SD [deg]	0.95	0.98	4.70	1.16	1.19	1.87
Loading direction = 90 deg						
Pretension [N]	9.47E+05	9.40E+05	8.39E+05	8.52E+05	8.45E+05	8.48E+05
Mooring tension, max [N]	2.45E+06	1.36E+06	4.29E+06	2.27E+06	1.20E+06	1.86E+06
Mooring tension, mean [N]	1.45E+06	6.24E+05	9.59E+05	1.33E+06	5.19E+05	9.59E+05
Mooring tension, SD [N]	2.16E+05	1.45E+05	5.29E+05	2.02E+05	1.16E+05	1.44E+05
Mooring angle, max [deg]	68.28	63.97	89.99	67.57	62.71	64.97
Mooring angle, mean [deg]	63.61	56.57	80.42	63.03	54.62	60.53
Mooring angle, SD [deg]	1.22	2.21	3.03	1.25	2.20	1.14

after reaching a static equilibrium, the two FOWTs of the baseline FOWF approach each other by approximately 2.5 m along the x_g-axis compared to their initial positions. This is caused by the self weight of the shared line, as explained in Section 2. For the mean dynamic positions, a large offset is observed in the loading direction, which is caused by the mean aerodynamic load and the mean wave drift force. Compared with the single FOWT, Spar 1 and Spar 2 have relatively larger motion ranges and standard deviations (SDs) with 0-deg loading direction and similar motion ranges and SDs with 90-deg loading direction. This observation is due to the shared line configuration (one shared line in the x_g-direction) of the baseline FOWF and is expected to change for other shared line configurations. The difference of the restoring force provided by Line 5 of the baseline FOWF and Line 3 of the single FOWT is important for the motions of FOWTs in the 0-deg loading direction, but the influence of the difference in the restoring force is not significant for the motions of FOWTs in the 90-deg loading direction because the line is nearly perpendicular to the loading direction.

5.1.3. Comparison of structural response

Among the structural response variables, the mooring tension and tower-base bending moment (TBBM) are selected as key indicators affected by the dynamics of the FOWTs. For each mooring line, the mooring tension and angle at the fairlead are of interest. The mooring angle is defined as the angle between the mooring line and the vertical direction at the fairlead. The sagging depth, $Z_{sagging}$, is investigated to study the line shape of the shared line under dynamic responses. $Z_{sagging}$ is defined as the vertical distance from the lowest point on the shared line to the SWL. $Z_{sagging}$ must be sufficiently large, e.g., > 20 m, if vessels are to pass between FOWTs.

The statistics of mooring tension and mooring angles at the fairleads are summarized in Table 7 for mooring lines connected to Spar 1 and Spar. The maximum value, mean value and SD presented in the table are averaged over 20 realizations. For the 0-deg loading direction, higher tension at the fairlead is observed for single lines of the baseline FOWF than for those of the single FOWT. This is because Spar 1 has a larger mean dynamic offset than Spar, as shown in Table 6. For the 90-deg loading direction, the mooring responses of Line 1 and Line 2 are comparable between Spar 1 and Spar. This is in agreement with the mean dynamic positions of FOWTs shown in Table 6. The maximum mooring angles at the fairlead Line 5 f1 are close to 90 deg for both loading directions, indicating a tightened shared line. It is observed that for both loading directions, the SDs of mooring tension and mooring angle at the fairlead are much higher in the shared line than in the single lines. This is the trade-off of the reduced number of single mooring lines and anchors. Therefore, the design of the shared line is of importance to avoid premature or cascade mooring failures of FOWFs in extreme ocean environments.

A snap event of a mooring line is characterized as a sharp tension spike whose magnitude exceeds typical values of local tension maxima, after a temporary slackness in the mooring line [26]:

$$T_{start} \leq 0.1 \cdot T_{static} \tag{2}$$

$$T_{end} \geq 1.9 \cdot T_{static} \tag{3}$$

where T_{start} is the local tension minima when the snap event starts; T_{end} is the local tension maxima when the snap event ends; T_{static} is the pretension plus the contribution caused by the mean environmental load, i.e., the mean dynamic mooring tension. Snap load events are checked for all mooring lines of the baseline FOWF. For the investigated loading directions, snap load events are only observed in the shared line. The shared line experiences more snap load events in the 0-deg loading direction than in the 90-deg loading direction due to larger relative surge motions between FOWTs. For twenty one-hour time-domain simulations, the averaged number of snap events observed at the fairlead Spar 1, Line 5 f1 is 209.35 for the 0-deg loading direction and 86.05 for the 90-deg

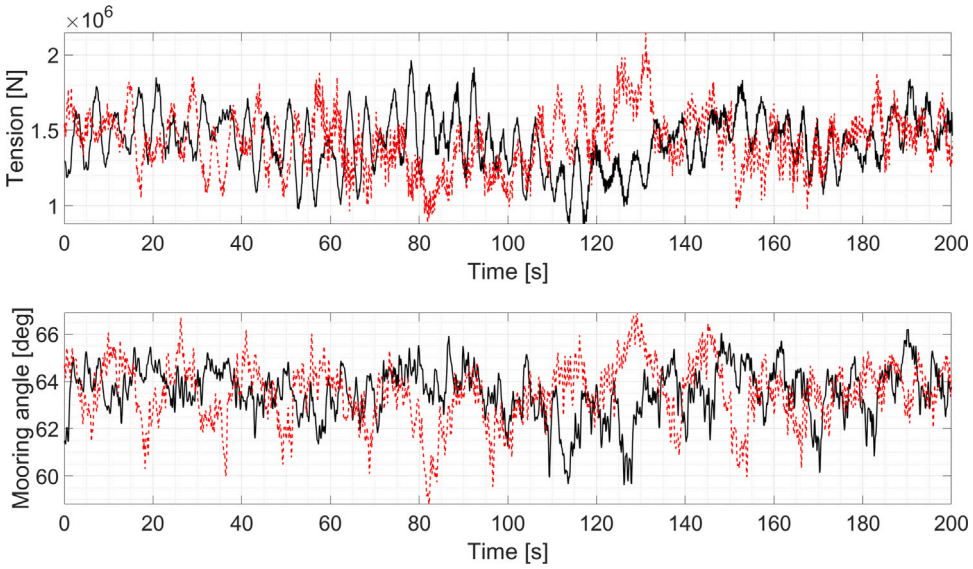

Fig. 7. Mooring response time series of Line 1 (solid line: 0 deg, dashed line: 90 deg).

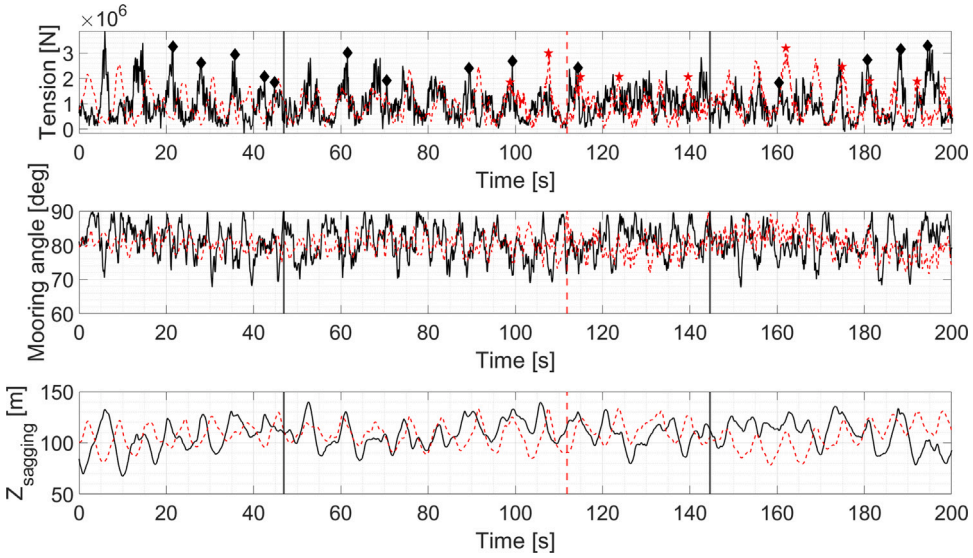

Fig. 8. Mooring response time series of Line 5 f1 (solid line: 0 deg, dashed line: 90 deg).

loading direction. For the realization with the closest platform motion SD to the mean SD over twenty realizations, the time series of mooring responses of Spar 1, Line 1 are plotted in Fig. 7; the time series of mooring responses of Spar 1, Line 5 f1 are plotted in Fig. 8 with T_{end} of snap load events marked in the time series of mooring tension. Smaller mooring tension with larger variation is found for Line 5 f1 compared with that for Line 1. Time instants where the mooring angle is close to 90 deg are marked with solid lines in Fig. 8. It is observed that the peaks of mooring tension and the mooring angle do not occur simultaneously.

TBBM is presented in the local coordinate system of the tower. In the initial condition, a positive fore-aft TBBM is about the negative y_g-axis and a positive side-side TBBM is about the positive x_g-axis (refer to Fig. 2(a)). The statistics of TBBM are summarized in Table 8 for the baseline FOWF and the single FOWT, in which the mean value and SD are averaged over twenty realizations. It is observed that in the loading direction, both Spar 1 and Spar 2 of the baseline FOWF have comparable TBBM statistics as the single FOWT does. This indicates that for the baseline FOWF with the shared mooring system, the structural design of the towers does not involve additional considerations.

Table 8
Statistics of TBBMs in the dynamic analyses.

Parameter	Baseline FOWF				Single FOWT	
	Spar 1 fore-aft	Spar 1 side-side	Spar 2 fore-aft	Spar 2 side-side	Spar fore-aft	Spar side-side
Loading direction = 0 deg						
TBBM, mean [Nm]	−2.43E+07	−2.95E+06	−2.18E+07	−8.88E+06	−2.48E+07	−2.86E+06
TBBM, SD [Nm]	5.59E+07	6.50E+06	5.57E+07	8.98E+06	5.58E+07	6.54E+06
Loading direction = 90 deg						
TBBM, mean [Nm]	4.09E+06	−7.47E+07	2.98E+06	−7.43E+07	3.56E+06	−7.44E+07
TBBM, SD [Nm]	4.06E+06	5.77E+07	3.95E+06	5.77E+07	2.44E+06	5.78E+07

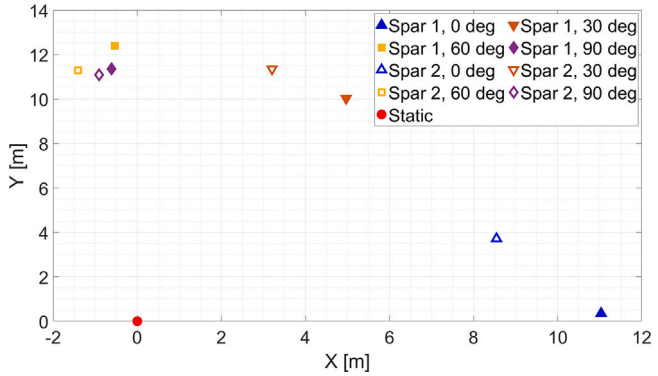

Fig. 9. Mean position of body origins of FOWTs in the horizontal plane due to variation of the loading direction.

5.2. Sensitivity study

In the following sections, results of the sensitivity study on the loading direction are presented in Section 5.2.1 and results of the sensitivity study on the shared line diameter are discussed in Section 5.2.2. In sensitivity studies, simulations and analyses are carried out for the dual-spar FOWF only.

5.2.1. Sensitivity study on the loading direction

As discussed in Section 4.3.1, dynamic analyses have been performed for the baseline FOWF in four loading directions, i.e., 0 deg, 30 deg, 60 deg and 90 deg. The linearized mooring stiffness, horizontal platform motions and structural response are investigated and discussed below.

Influence on linearized mooring stiffness

As mentioned in Section 5.1.1, for the investigated loading directions, the mooring stiffness is linearized around the mean dynamic position in the coordinate system where the x-axis is along the loading direction. The results are presented in Fig. 6 with markers. For the baseline FOWF, large variations with respect to the loading direction are observed in both the stiffness terms "C_{M11}, dual, dynamic" and "C_{M77}, dual, dynamic". This is caused by different mean dynamic positions of FOWTs due to mean environmental loads under environmental conditions with different loading directions. For each investigated loading direction, the stiffness term "C_{M11}, dual, dynamic" of Spar 1 is different from the stiffness term "C_{M77}, dual, dynamic" of Spar 2, which indicates that unlike the static condition, Spar 1 and Spar 2 are expected to show different motion characteristics in the dynamic analyses. The linearized mooring stiffness is plotted for the single FOWT for comparison. The stiffness term "C_{M11}, dual, dynamic" of Spar 1 and the stiffness term "C_{M11}, single, dynamic" of Spar show similar variations with respect to the loading directions, resulting from similar mooring layouts as shown in Figs. 2(a) and 4.

Influence on platform motion in the horizontal plane

The mean dynamic positions of FOWTs averaged over 20 realizations are plotted in Fig. 9, in which the static equilibrium positions of FOWTs are taken as the reference and put at the original point. Therefore, Fig. 9 presents how far the mean dynamic positions of Spar 1 and Spar 2 move from the static condition in different loading directions. The mean dynamic positions have contributions from both the mean aerodynamic load and the mean wave drift force. The magnitude of the mean wave drift force is on the same level with respect to loading directions, while the mean aerodynamic load differs. The statistics of aerodynamic force acting on the FOWTs are plotted in Fig. 10 with respect to the variation of the loading direction. In Fig. 10, the aerodynamic force is presented in the main shaft coordinate system. The x-shaft-axis is along the shaft line and the y-shaft-axis is perpendicular to the shaft line and in the same direction as the y_g-axis in the initial condition. As described in Section 4.1, the blades of the FOWTs are feathered. Therefore, the mean angles of attack of the blades increase with the increasing loading direction. When the loading direction is 0 deg, the blades are parallel to the main wind direction, and the drag forces acting on the blades are small which leads

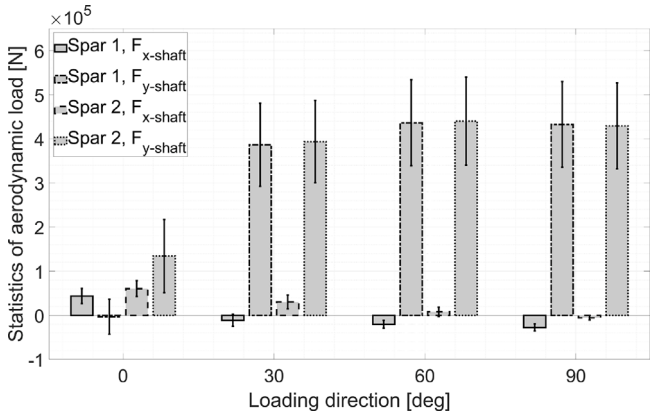

Fig. 10. Statistics of aerodynamic force acting on the FOWTs due to variation of the loading direction (bar: mean value averaged over realizations, error bar: SD averaged over realizations).

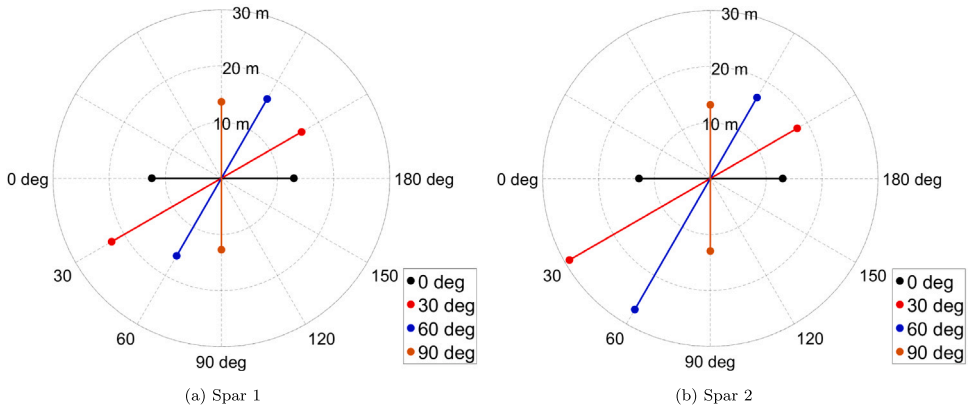

Fig. 11. Platform motion range of FOWTs in the loading direction due to variation of the loading direction.

to small aerodynamic forces in the x-shaft direction. When the loading direction is 90 deg, the drag forces acting on the blades are large which results in large aerodynamic forces in the y-shaft direction. In Fig. 9, it is observed that with the 0-deg loading direction, Spar 2 has a mean offset perpendicular to the loading direction. This is explained by the aerodynamic force acting on Spar 2 in the y-shaft direction, as shown in Fig. 10. From Figs. 9 and 10, it is seen that the component of aerodynamic force acting in the y-shaft direction is positively correlated to the mean offset of FOWTs in the y_g direction.

The platform motion ranges in the loading direction are averaged over the realizations and plotted in Fig. 11 with respect to different loading directions. It is observed that Spar 2 has larger motion ranges than Spar 1 in the 30-deg and 60-deg loading directions. This interesting observation is explained by the mooring stiffness linearized about the mean dynamic positions, shown in Fig. 6. In the 30-deg and 60-deg loading directions, the stiffness terms "C_{M77}, dual, dynamic" are much smaller than "C_{M11}, dual, dynamic".

Influence on structural response

Statistics of mooring responses are plotted in Fig. 12 with respect to the variation of the loading direction.

In Fig. 12(a), it is observed that Line 1 and Line 4 are more loaded than the rest single lines in loading directions except for the 0-deg loading direction. This can be explained by the mean dynamic positions of FOWTs shown in Fig. 9. The windward single lines are expected to be more loaded than the leeward single lines. When the loading direction is 0 deg, Spar 1 and Spar 2 are driven to move along the x_g axis. Therefore, the windward single lines, Line 1 and Line 2, are the most loaded. For Line 4, the averaged maximum mooring tension is over the minimum breaking strength (MBS) for the 30-deg loading direction and close to the MBS for the 60-deg loading direction, resulting from the large platform motion ranges in these two loading directions shown in Fig. 11(b). It is noticed that although the mean tension in the shared line is not necessarily higher than those in the single lines, the variation of the mooring tension is the most significant. This is caused by the relative motions between Spar 1 and Spar 2. The shared line is tightened and loosened back-and-forth because of the dynamic motions of the two FOWTs. Due to the large motion ranges of both FOWTs shown in Fig. 11, the maximum mooring tension experienced by the shared line is close to the MBS in the 30-deg and 60-deg loading directions, indicating the necessity of a redesign for the shared line.

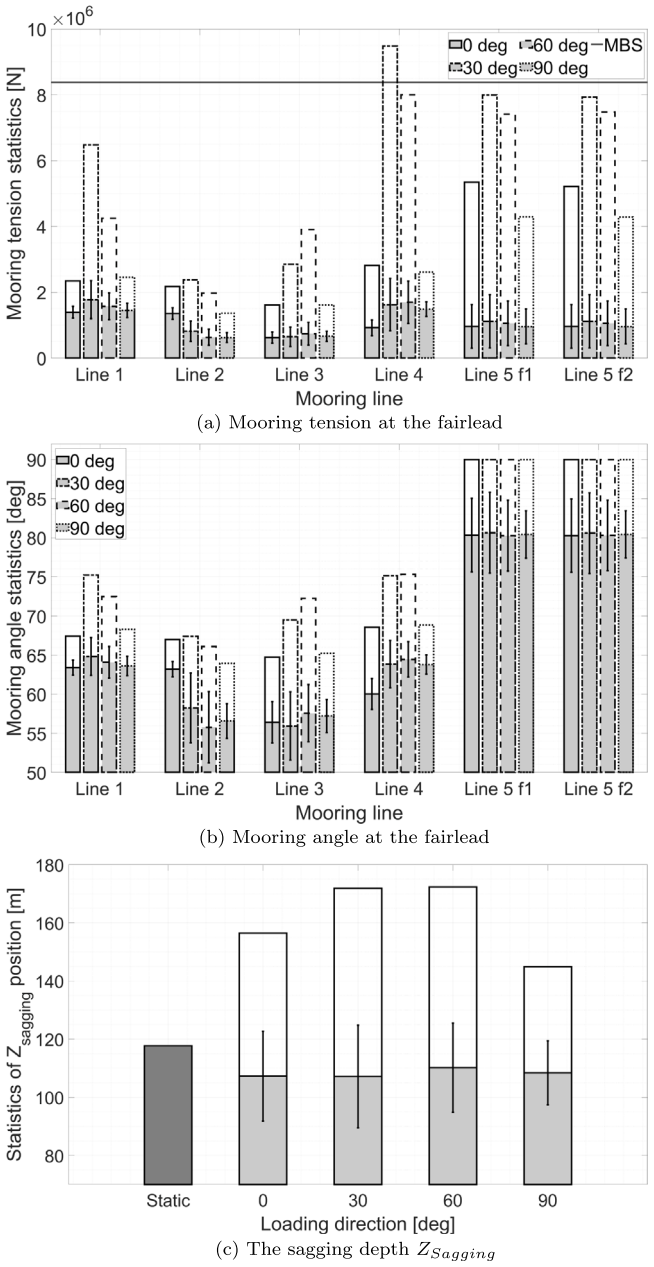

(a) Mooring tension at the fairlead

(b) Mooring angle at the fairlead

(c) The sagging depth $Z_{Sagging}$

Fig. 12. Statistics of mooring responses due to variation of the loading direction (gray bar: mean value averaged over realizations, white bar: maximum value averaged over realizations, error bar: SD averaged over realizations).

In Fig. 12(b), it is found that Line 1 and Line 4 have larger mean and maximum mooring angles while Line 2 and Line 3 have larger SDs of the mooring angle. This is due to the mean dynamic positions and the motion ranges of FOWTs, as shown in Figs. 9 and 11. The more loaded windward single lines have larger mean and maximum mooring angles and the less loaded leeward single lines have larger variations of mooring angles. The shared line has a large mean mooring angle as expected. For all investigated loading directions, the shared line is tightened when the mooring angle reaches 90 deg. Therefore, additional attention should be paid to the design of the shared line. Clump weights or alternative material compositions may be considered in the design of the shared line to alter the line shape and to reduce the tension variations.

From Fig. 12(c), it is seen that the sagging depth has the largest mean value in the static equilibrium, while in dynamic analyses, the mean sagging depth is smaller due to the relative motion of FOWTs. For different loading directions, the difference in the mean sagging depth is not significant. A positive correlation is found between the platform motion ranges of FOWTs shown in Fig. 11(b) and the maximum and the SD of the sagging depth of the shared line shown in Fig. 12(c) as the maximum and the SD of the sagging

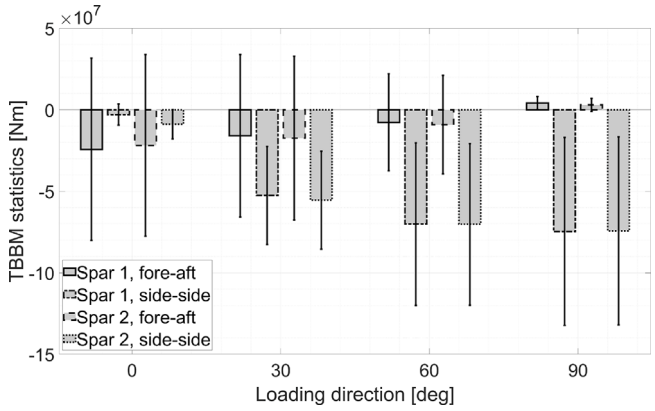

Fig. 13. Statistics of TBBM due to the variation of the loading direction (bar: mean value averaged over realizations, error bar: SD averaged over realizations).

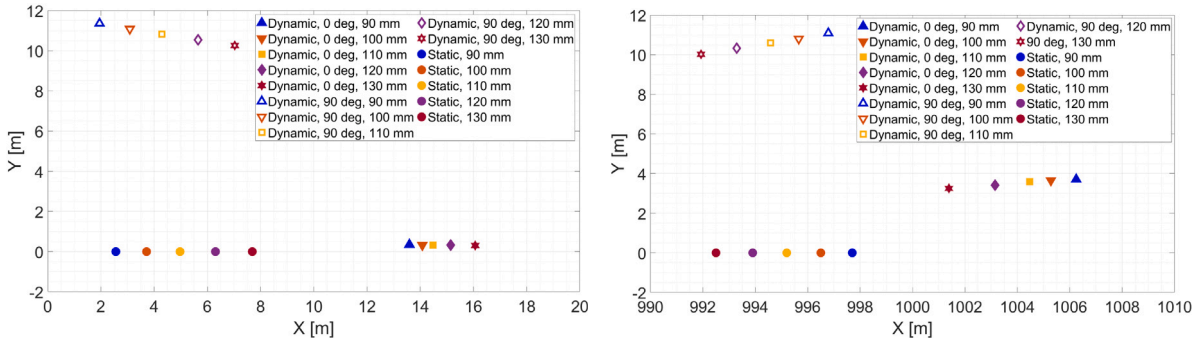

(a) Spar 1 (b) Spar 2

Fig. 14. Mean positions of body origins of FOWTs in the horizontal plane due to variation of the shared line diameter.

depth depends on the level of relative motions between FOWTs. This sagging depth can potentially affect the vessels passing between the FOWTs.

Statistics of TBBM are plotted in Fig. 13 with respect to the loading directions. It is observed that with an increasing loading direction, the fore-aft TBBMs of both FOWTs decrease and the side-side TBBMs increase. This is in agreement with the variation of aerodynamic forces acting on the FOWTs, as shown in Fig. 10.

5.2.2. Sensitivity study on the shared line diameter

As mentioned in Section 4.3.2, to investigate the influence of the shared line, dynamic analyses have been performed for the dual-spar configuration with different shared line diameters presented in Table 5. Two loading directions, 0 deg and 90 deg are considered. The results are discussed in the following sections.

Influence on linearized mooring stiffness

The mean dynamic positions of FOWTs are averaged over all realizations and plotted in Fig. 14 with respect to dual-spar configurations with different shared line diameters. The static equilibrium positions of body origins of FOWTs are marked in the plot as well. Because the total length of the shared line remains fixed, the self weight of the shared line is proportional to the diameter. The shared line is heavier with a larger diameter, and the two FOWTs are drawn closer to each other under the static equilibrium. As shown in Fig. 14, the variation trend of the mean position of the two FOWTs with regard to the shared line diameter remains the same in both dynamic and static conditions.

The mooring stiffness is linearized for the dual-spar configurations with different shared line diameters. The linearization procedures described in Section 5.1.1 have been applied. The linearized mooring stiffness terms in the loading direction, C_{M11} and C_{M77}, are plotted in Fig. 15 with respect to different shared line diameters.

For the 0-deg loading direction, the shared line is heavier with a larger diameter and two FOWTs are closer to each other in the x_g direction under the static equilibrium, shown in Fig. 14. The mooring tension at the fairleads is affected in both single lines and the shared line. As a result, the increase of the shared line diameter leads to a decrease in the mooring stiffness linearized about the static positions. The variation of the linearized mooring stiffness, "$C_{M11/77}$, 0 deg, static", is around 28%. Due to the mean aerodynamic load acting on FOWTs in the dynamic condition, both Spar 1 and Spar 2 are driven along the x_g direction as

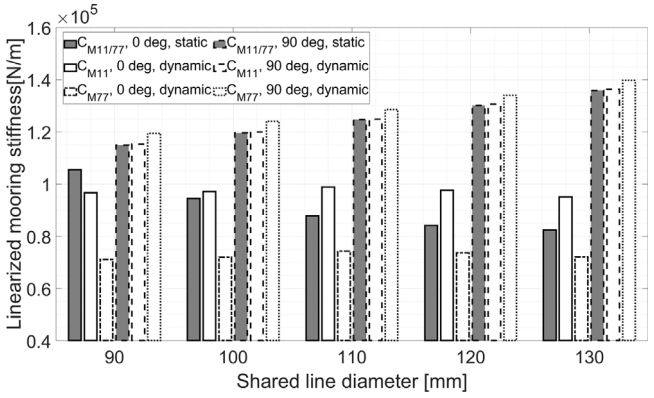

Fig. 15. Linearized mooring stiffness for dual-spar FOWFs with different shared line diameters.

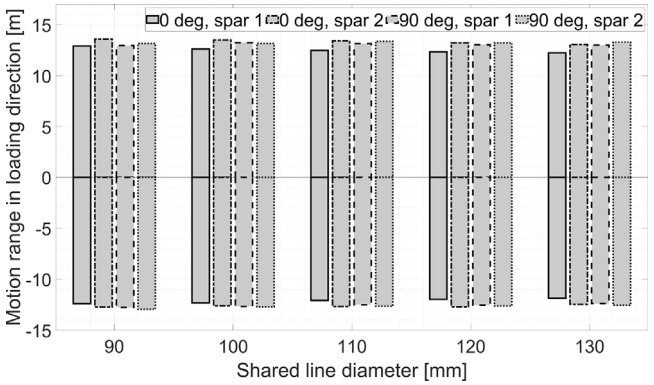

Fig. 16. Mean platform motion range of FOWTs in the loading direction due to variation of the shared line diameter.

shown in Fig. 14. Two single lines connected to Spar 1 are stretched more and two single lines connected to Spar 2 are stretched less. Therefore, the linearized mooring stiffness of Spar 1 is larger than that of Spar 2 in the dynamic condition. For the 0-deg loading direction, the influence of the shared line diameter is less significant on the linearized mooring stiffness in the dynamic case compared to that in the static case. The variation of the linearized mooring stiffness, "C_{M11}, 0 deg, dynamic" and "C_{M77}, 0 deg, dynamic" due to the variation of the shared line diameter is less than 5%.

For the 90-deg loading direction, the mooring tension in the shared line is nearly perpendicular to the loading direction in both static and dynamic cases. The major influence on the variation of the linearized mooring stiffness is dominated by the single lines connected to the FOWTs. As shown in Fig. 14, a shared line with a larger diameter drives two FOWTs closer towards each other and tightens the single lines more. Therefore, the linearized mooring stiffness rises with increasing shared line diameter for both FOWTs. From Fig. 15, the variation of the linearized mooring stiffness in the 90-deg loading direction is around 18%.

Influence on platform motion in the horizontal plane

The horizontal platform motion range in the loading direction is averaged over realizations and plotted in Fig. 16 with respect to the shared line diameter. The largest variation of the horizontal platform motion range is 5.5% in Fig. 16, which is relatively small considering the variation of the shared line diameter. The finding is in agreement with the observations for the linearized mooring stiffness presented in Fig. 15.

Influence on structural response

Statistics of mooring tension are plotted in Fig. 17 for the dual-spar configurations with different shared line diameters. From Figs. 17(a) and 17(b), it is observed that the influence of the shared line diameter on the pretension of the mooring lines is significant. The variation of pretension is approximately 23% for the single lines and 30% for the shared line. For the shared line, the pretension increases along with the shared line diameter due to the self weight of the shared line. For the single lines, the variation of the pretension is caused by the static equilibrium positions of FOWTs. The single lines are stretched more when two FOWTs are closer to each other with a heavier shared line, as shown in Fig. 14. For different loading directions, the windward single lines are more loaded than the leeward single lines, as shown in Figs. 17(c) and 17(d). Due to the relative motions of the FOWTs, significant variations of mooring tension are found in the shared line, which should be considered in the design of the shared line. For both loading directions, the mean mooring tension is higher in all mooring lines with a larger shared line diameter. This is expected because a

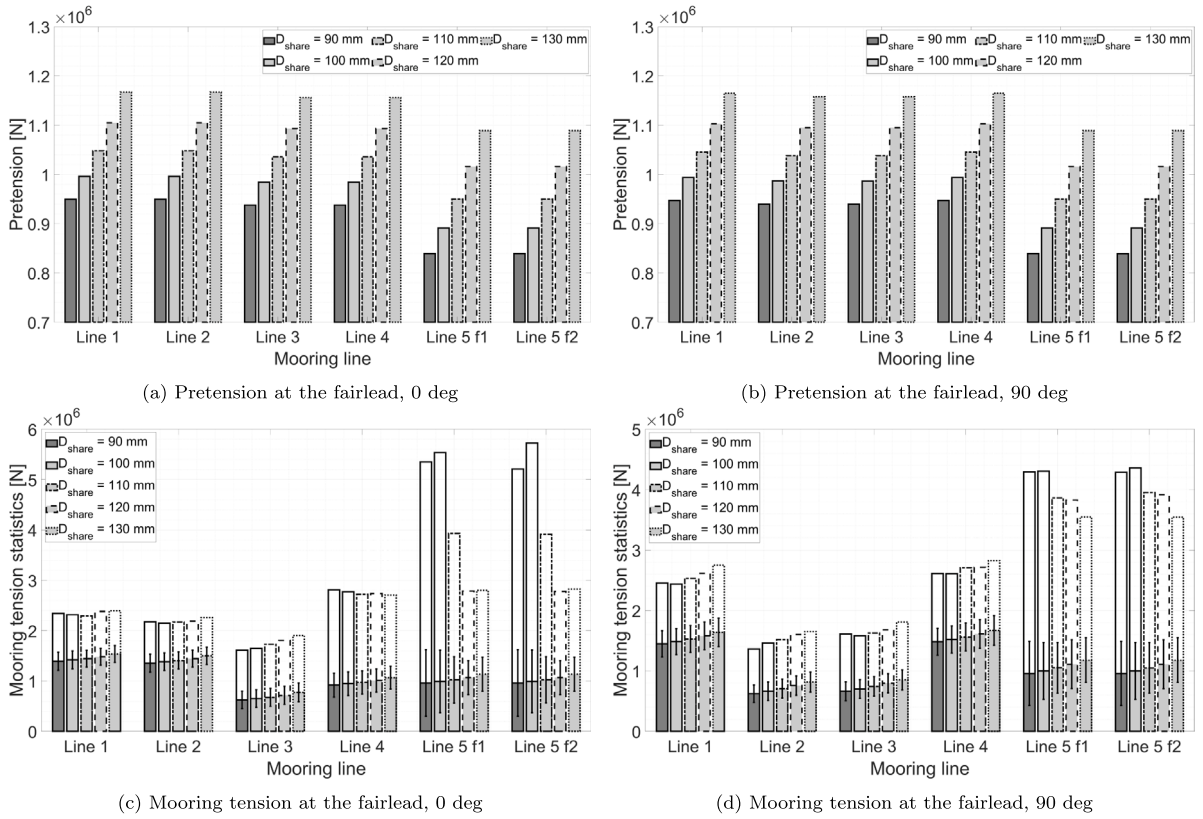

(a) Pretension at the fairlead, 0 deg

(b) Pretension at the fairlead, 90 deg

(c) Mooring tension at the fairlead, 0 deg

(d) Mooring tension at the fairlead, 90 deg

Fig. 17. Statistics of mooring tension due to variation of the shared line diameter (gray bar: mean value averaged over realizations, white bar: maximum value averaged over realizations, error bar: SD averaged over realizations).

heavier shared line results in higher mean tension in the shared line, and the fairleads of single lines are farther from the anchors, which increases the mean tension in the single lines as well. For the two loading directions, though the pretension in the shared line increases with the increasing shared line diameter, the maximum mooring tension in the shared line decreases. All the maximum tension in Figs. 17(c) and 17(d) is below the MBS presented in Table 5. The analysis of snap load events described in Section 5.1.3 has been performed in this sensitivity study as well. With the increasing shared line diameter, the averaged number of snap events observed at the fairlead Spar 1, Line 5 f1 decreases from 209.35 to 3.20 for the 0-deg loading direction and decreases from 86.05 to 5.50 for the 90-deg loading direction, which shows a similar variation trend as the maximum mooring tension presented in Figs. 17(c) and 17(d).

Statistics of the mooring angles and sagging depth are plotted in Fig. 18 for the dual-spar FOWF with different shared line diameters. From Figs. 18(a) and 18(b), it is observed that the mean mooring angles of all single lines increase along with the shared line diameters. The mooring properties of single lines are not changed in the sensitivity study. With an increasing shared line diameter, the FOWTs move towards each other and the fairleads move away from the anchors. Therefore, the mean mooring angles increase accordingly. The line shape of a shared line in the static condition has been studied in [9] for different materials and diameters. It is found that the mooring angle of the shared line decreases with increasing diameter. This is observed in the dynamic condition as well, shown in Figs. 18(a) and 18(b) for the mean and the maximum mooring angles. From Fig. 18(c), in the static condition, the sagging depth of the shared line increases with the increasing shared line diameter, as discussed in [9]. In the dynamic condition, the maximum sagging depth and the mean sagging depth increase with the increasing shared line diameter while the SD of the sagging depth decreases. Therefore, if the sagging depth of the shared line may potentially affect the vessels passing through the FOWF, heavier shared lines with larger diameters should be considered.

Statistics of the TBBM due to the variation of the shared line diameter are investigated as well. It is found that the TBBMs of FOWTs are not sensitive to the shared line diameter, which makes the TBBMs less important in the design of the shared line. For the shared line diameters and loading directions investigated, the variations of all TBBMs are less than 4%.

6. Conclusion

This paper presents a dynamic analysis of a dual-spar floating offshore wind farm (FOWF) with a shared mooring system in extreme environmental conditions. To investigate the influence of the shared mooring on the system behavior, a baseline FOWF is

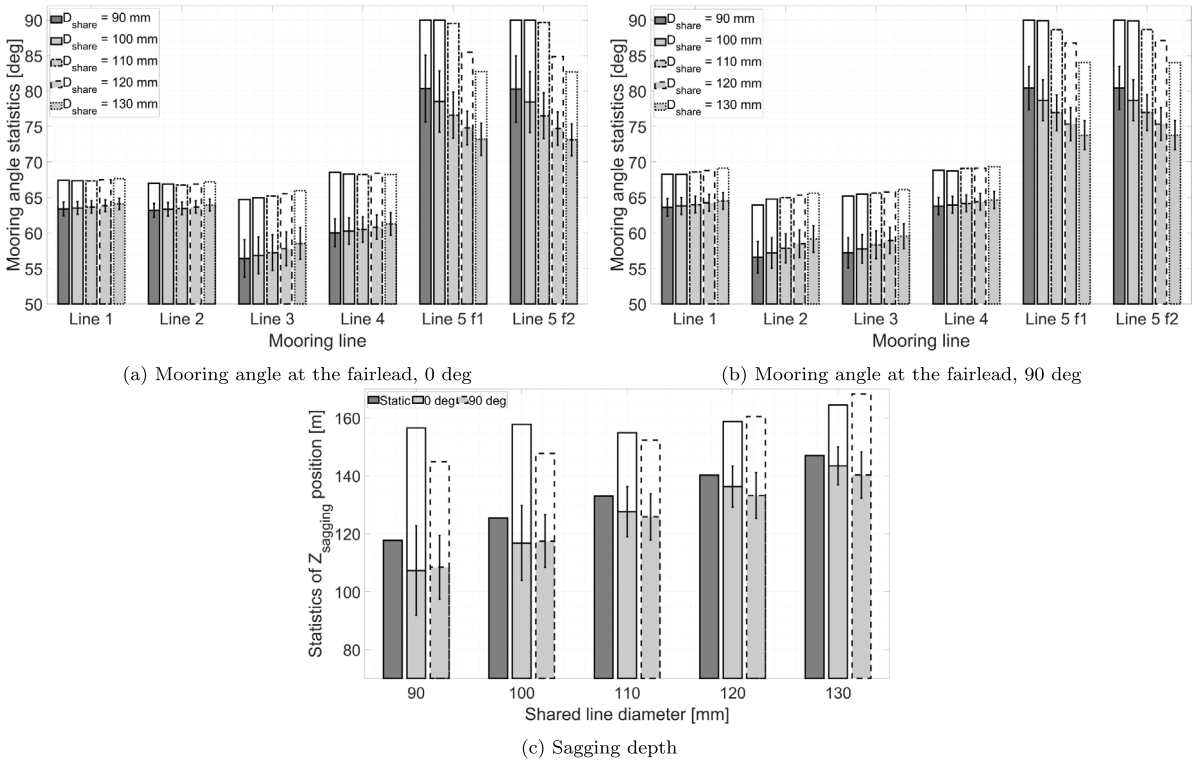

(a) Mooring angle at the fairlead, 0 deg

(b) Mooring angle at the fairlead, 90 deg

(c) Sagging depth

Fig. 18. Statistics of mooring angles and sagging depth due to variation of the shared line diameter (gray bar: mean value averaged over realizations, white bar: maximum value averaged over realizations, error bar: SD averaged over realizations).

numerically modeled followed by a detailed case study. Metocean conditions with a 50-year return period are considered and the platform motion and structural responses of the baseline FOWF are compared to those of a single floating offshore wind turbine (FOWT). Then, a sensitivity study is performed to assess the influence of different loading directions and shared line diameters. The main conclusions of this paper are as follows:

- Compared to the single FOWT, larger horizontal platform motions of FOWTs and higher mooring tension in single lines are found for the dual-spar FOWF. Although the tension level is below the minimum breaking strength in the simulations, large tension variations and snap events are experienced by the shared line. The design should address snap load events considering the consequences of snap loads including line breakage and loss of a turbine.
- It is seen that the loading direction has a significant influence on the platform motions of the FOWTs. The present mooring system layout with one shared line contributes to the variation of station-keeping performance in different directions. The directional dependence of other FOWF layouts, such as four FOWTs arranged in a square, may exhibit different trends. For different loading directions, the windward single lines are more loaded than the leeward single lines. The sagging depth of the shared line experiences large variations up to 16% of the mean sagging depth in dynamic simulations with different loading directions. For shared mooring applications with small static sagging depth, the potential effects on the passing vessels should be taken into account in the design of the shared mooring system.
- From the sensitivity study, it is found that the horizontal platform motions and the tower-base bending moments are not sensitive to the shared line diameter. The influence of the shared line diameter is observed on the mooring responses. In the sensitivity study, the variation of the pretension is approximately 23% for the single lines and 30% for the shared line. It is also demonstrated that the shared line diameter has a strong effect on the likelihood of snap loads because the number of snap events drops dramatically as the shared line diameter increases.

7. Limitations and future work

This paper is limited to a dual-spar FOWF. In future, it would be interesting to investigate the dynamics of FOWFs with additional wind turbines and alternative shared mooring system configurations. It is also of interest to study the dynamic behaviors of the baseline FOWF under operational loading conditions, and further, to explore the influence of the shared mooring configuration on the structural fatigue life. As the natural periods of the FOWF with a shared mooring system are quite different from those of the original OC3 Hywind spar FOWT [27], the controllers used in operational conditions need to be tuned properly so that

the control algorithm can provide enhanced damping control at multiple resonant frequencies experienced by the FOWF with the shared mooring [28–31]. In addition, if the FOWTs are too close to each other during operation, the aerodynamic interactions must be addressed in numerical simulations. For the design check of the fatigue limit state, different load cases need to be considered together with their probabilities of occurrence [32,33].

As shared lines connect adjacent FOWTs and integrate the FOWF as one floating system, it is of interest to study the failure of the shared mooring system. Risk assessments and consequence analysis of different mooring failure scenarios, especially in the case of a cascade failure, should be addressed in future work.

Declaration of competing interest

The authors declare that they have no known competing financial interests or personal relationships that could have appeared to influence the work reported in this paper.

Data availability

Data will be made available on request.

Acknowledgments

The authors acknowledge the financial support from the Norwegian Ministry of Education and Research granted through the Department of Engineering Sciences, University of Agder.

References

[1] Yamamoto S, Colburn Jr WE. Power generation assemblies. 2005, International Patent, Publication Number W0 2005/040604 A2.
[2] Hill JS. Hywind Scotland, world's first floating wind farm, performing better than expected, Vol. 16. Sustainable Enterprises Media, Inc; 2018.
[3] Goldschmidt M, Muskulus M. Coupled mooring systems for floating wind farms. Energy Procedia 2015;80:255–62.
[4] Hall M, Connolly P. Coupled dynamics modelling of a floating wind farm with shared mooring lines. In: ASME 2018 37th international conference on ocean, offshore and arctic engineering, Madrid, Spain. American Society of Mechanical Engineers Digital Collection; 2018.
[5] Connolly P, Hall M. Comparison of pilot-scale floating offshore wind farms with shared moorings. Ocean Eng 2019;171:172–80.
[6] Hall M. MoorDyn V2: New capabilities in mooring system components and load cases. Technical report, Golden, CO (United States): National Renewable Energy Lab. (NREL); 2020.
[7] Wilson S, Hall M, Housner S, Sirnivas S. Linearized modeling and optimization of shared mooring systems. Ocean Eng 2021;241:110009.
[8] Munir H, Lee CF, Ong MC. Global analysis of floating offshore wind turbines with shared mooring system. In: IOP conference series: materials science and engineering, Vol. 1201. IOP Publishing; 2021, 012024.
[9] Liang G, Merz K, Jiang Z. Modeling of a shared mooring system for a dual-spar configuration. In: International conference on offshore mechanics and arctic engineering, volume 9: Ocean renewable energy. American Society of Mechanical Engineers; 2020.
[10] Liang G, Jiang Z, Merz K. Mooring analysis of a dual-spar floating wind farm with a shared line. J Offshore Mech Arct Eng 2021;143(6):062003.
[11] Jonkman J, Butterfield S, Musial W, Scott G. Definition of a 5-MW reference wind turbine for offshore system development. Technical report NREL/TP-500-38060, Golden, CO (United States): National Renewable Energy Lab. (NREL); 2009.
[12] Jonkman J. Definition of the floating system for phase IV of OC3. Technical report NREL/TP-500-47535, Golden, CO (United States): National Renewable Energy Lab. (NREL); 2010.
[13] DNV GL. Offshore standard DNVGL-OS-E301, position mooring. Høvik, Norway; 2015.
[14] SINTEF Ocean. SIMO 4.16.0 user guide. Trondheim, Norway; 2019.
[15] SINTEF Ocean. RIFLEX 4.16.0 user guide. Trondheim, Norway; 2019.
[16] DNV GL. SESAM user manual, wave analysis by diffraction and Morison theory. Høvik, Norway; 2019.
[17] Liang G, Jiang Z, Merz K. Influence of aerodynamic loads on a dual-spar floating offshore wind farm with a shared line in parked conditions. In: International conference on offshore mechanics and arctic engineering, Vol. 85932. American Society of Mechanical Engineers; 2022, V008T09A023.
[18] DNV. Recommended practice DNV-RP-C205, environmental conditions and environmental loads. Høvik, Norway; 2010.
[19] DNV. Standard DNV-ST-0119, floating wind turbine structures. Høvik, Norway; 2018.
[20] Li L, Gao Z, Moan T. Joint distribution of environmental condition at five European offshore sites for design of combined wind and wave energy devices. J Offshore Mech Arct Eng 2015;137(3).
[21] IEC. International standard IEC 61400-1, wind turbines—Part 1: Design requirements. Geneva, Switzerland; 2005.
[22] IEC. International standard IEC 61400-3, wind turbines—Part 3: Design requirements for offshore wind turbines. Geneva, Switzerland; 2009.
[23] Jonkman BJ, Buhl Jr ML. TurbSim user's guide. Technical report, Golden, CO (United States): National Renewable Energy Lab. (NREL); 2006.
[24] Ikhennicheu M, Lynch M, Doole S, Borisade, et al. Review of the state of the art of mooring and anchoring designs, technical challenges and identification of relevant DLCs. 2021.
[25] Stevens RJ, Gayme DF, Meneveau C. Effects of turbine spacing on the power output of extended wind-farms. Wind Energy 2016;19(2):359–70.
[26] Hsu W-t, Thiagarajan KP, Manuel L. Extreme mooring tensions due to snap loads on a floating offshore wind turbine system. Mar Struct 2017;55:182–99.
[27] Jonkman J, Larsen T, Hansen A, Nygaard T, Maus K, Karimirad M, Gao Z, Moan T, Fylling I. Offshore code comparison collaboration within IEA wind task 23: Phase IV results regarding floating wind turbine modeling. Technical report, Golden, CO (United States): National Renewable Energy Lab. (NREL); 2010.
[28] Larsen TJ, Hanson TD. A method to avoid negative damped low frequent tower vibrations for a floating, pitch controlled wind turbine. In: Journal of physics: conference series, Vol. 75. IOP Publishing; 2007, 012073.
[29] Nielsen FG, Skaare B, Tande JOG, Norheim I, Uhlen K. Method for damping tower vibrations in a wind turbine installation. 2012, US Patent 8, 186, 949.
[30] Skaare B, Nielsen FG, Hanson TD, Yttervik R, Havmøller O, Rekdal A. Analysis of measurements and simulations from the hywind demo floating wind turbine. Wind Energy 2015;18(6):1105–22.
[31] Merz K. Basic controller tuning for large offshore wind turbines. Wind Energy Sci 2016;1(2):153–75.
[32] DNV. Recommended practice DNV-RP-0286, coupled analysis of floating wind turbines. Høvik, Oslo, Norway; 2019.
[33] ABS. Guidance notes on global performance analysis for Floating Offshore wind turbines installations. Houston (TX), USA; 2020.